JOURNAL OF MATERIALS SCIENCE **36** (2001) 2371–2381

Characterization of nearly stoichiometric SiC ceramic fibres

S. M. DONG
Laboratoire des Composites Thermostructuraux (LCTS), UMR 5801 (CNRS-SNECMA-CEA-UB1), 3 allée de La Boétie, domaine universitaire, 33600 Pessac, France; Shanghai Institute of Ceramics, Chinese Academy of Sciences, 200050 Shanghai, People's Republic of China

G. CHOLLON*
Laboratoire des Composites Thermostructuraux (LCTS), UMR 5801 (CNRS-SNECMA-CEA-UB1), 3 allée de La Boétie, domaine universitaire, 33600 Pessac, France
E-mail: chollon@lcts.u-bordeaux.fr

C. LABRUGÈRE, M. LAHAYE
Centre de Caractérisation des Matériaux Avancés (CeCaMA), ICMCB, avenue du Dr A. Schweitzer, 33600 Pessac, France

A. GUETTE
Laboratoire des Composites Thermostructuraux (LCTS), UMR 5801 (CNRS-SNECMA-CEA-UB1), 3 allée de La Boétie, domaine universitaire, 33600 Pessac, France; Centre de Caractérisation des Matériaux Avancés (CeCaMA), ICMCB, avenue du Dr A. Schweitzer, 33600 Pessac, France

J. L. BRUNEEL, M. COUZI
Laboratoire de Physico-Chimie Moléculaire (LPCM), UMR 5803, 351, cours de la Libération, 33405 Talence, France

R. NASLAIN
Laboratoire des Composites Thermostructuraux (LCTS), UMR 5801 (CNRS-SNECMA-CEA-UB1), 3 allée de La Boétie, domaine universitaire, 33600 Pessac, France

D. L. JIANG
Shanghai Institute of Ceramics, Chinese Academy of Sciences, 200050 Shanghai, People's Republic of China

A comparative study of the chemical composition and microstructure of Hi-Nicalon, Hi-Nicalon type S, Tyranno SA, Sylramic and Carborundum fibres has been conducted. This analysis has confirmed results already published but has also evidenced some original features. The Hi-Nicalon type S fibre has a near stoichiometric composition but it still contains some oxygen (≈1 at. %) and free carbon (≈2 at. %). The expected near stoichiometric composition of both the Tyranno SA and the Sylramic fibres is only effective near the edge region, while the core of the fibres contains some amount of free carbon (e.g., up to ≈14 at. % and ≈6 at. % respectively in large diameter fibres) as well as some residual oxygen (≈0.5 at. %). The composition of the Carborundum fibre is very close to stoichiometric SiC except rare and localised free carbon or B_4C inclusions. The properties of the different fibres, some of them still beeing at a development stage, are discussed from a chemical and a phase composition point of view, on the basis of what is known about their respective preparation process.

1. Introduction

SiC fibres, which have many attractive intrinsic properties such as high tensile strength and high elastic modulus, high creep and oxidation resistance, are promising candidates for reinforcing ceramic matrix composites (CMC).

A fine diameter SiC-based fibre (Nicalon NL 200) has been commercialised since the late 70's by Nippon

* Author to whom all correspondence should be addressed.

Carbon Co., Yokohama, Japan (NC). This fibre is thermodynamically unstable at high temperature because of the silicon oxycarbide phase it contains [1–3]. This amorphous Si-C-O phase decomposes beyond 1100–1200°C, with a $SiO_{(g)}$ and $CO_{(g)}$ evolution and SiC crystal growth [4, 5]. This decomposition yields a highly porous structure and hence, a significant degradation of the strength and the elastic modulus of the fibres starting from 1100–1200°C [6–8]. To avoid the thermal instability due to the presence of the oxycarbide phase, specific processes have been developed to lower the oxygen content of the fibres and improve their high temperature resistance.

In 1990, a nearly oxygen-free Si-C fibre (Hi-Nicalon fibre from Nippon Carbon) was developed from the melt spinning, the electron beam curing and the pyrolysis of a polycarbosilane precursor (PCS) under anaerobic conditions [9–11]. This fibre has a much higher thermal stability than the standard Nicalon fibre. However, the Hi-Nicalon fibre not only consists of SiC nanocrystals but it also contains a large excess of turbostratic carbon which affects the oxidation and the creep resistance of the Hi-Nicalon fibre, with respect to stoichiometric SiC [12–16].

To reduce the free carbon content and eventually improve the high temperature properties of the fibres, much efforts have been devoted to develop near stoichiometric Si-C fibres. Those "third generation advanced fibres", include the Hi-Nicalon type S fibre from Nippon Carbon Co. [13–16], the recently developed Tyranno fibres from Ube Industries Ltd. (Ube, Japan) [17–20], the Sylramic SiC fibre from Dow-Corning Co. (Midland, USA) [21, 22]. One also should mention a relatively "old" stoichiometric α-SiC sintered fibre produced by Carborundum Co. (Niagara Falls, USA) [23, 24].

The information available on the processing routes to the standard and type S Hi-Nicalon fibres, tends to support the use of a common polycarbosilane (PCS) precursor as well as common spinning and electron beam curing processes [15]. The Hi-Nicalon S consists of β-SiC sub-micrometer crystals and also contains a very low carbon excess as well as traces of oxygen. Its stoichiometric character and coarse microstructure arise from a distinct pyrolysis process, i.e., under a specific atmosphere and at a higher temperature [13–16]. This fibre exhibits a high Young's modulus, a high creep and oxidation resistance and an excellent thermal stability up to 1600°C [14, 16].

The Tyranno family fibres, are originally produced by the reaction of PCS with a metal (M = Ti, Zr or Al) complex compound or alkoxide, its melt-spinning, curing and pyrolysis [17–20]. The Si-M-C-O Tyranno fibres containing metal additive have improved thermal stability and chemical corrosion resistance. However, the degradation of these fibres still occurs at high temperature (>1300°C) through a decomposition process due to their residual oxygen content. To improve their high temperature properties, the further heat treatment of an amorphous Si-Al-C-O fibre at about 1800°C has been conducted. The new Si-Al-C fibre (so-called Tyranno SA) shows no significant degradation in strength nor change in composition on heating up to 1800°C in argon (1 h) and up to 1000 h in air at 1000°C [18–20].

The Sylramic SiC fibre, is a boron-doped, fully crystallised fibre. This fibre is also a polymer-derived SiC fibre in which boron, serving as a sintering aid, is incorporated, allowing the carbothermic reduction to occur without forming a porous or excessively large-grained structure during the densification [21, 22]. The Sylramic fibre exhibits a high stiffness and a high thermal, creep and oxidation resistance [21, 22, 25].

The Carborundum sintered α-SiC fibre is prepared by extruding a viscous compound formed by mixing a sinterable submicrometer α-SiC powder and sintering additives (e.g., B and C) in a suitable polymeric binder [23, 24]. The extruded fibres are sintered at a temperature over 2000°C to reach full densification. The strength of this fibre is limited by the flaws resulting from the relatively large SiC grain and pore size [23]. This fibre is reported to have the best creep resistance of all the polycrystalline ceramic fibres fabricated to date [25]. It is however no longer produced.

All these fibres are characterised by a high density, a high tensile strength and Young's modulus and a relatively low fracture strain. Such room temperature features together with reported high temperature properties, make them suitable for reinforcing high performance CMC [26].

The objective of this study was to conduct a systematic and comparative study of the chemical composition and the microstructure of the series of advanced SiC fibres. Most of the chemical and microstructural investigations performed up to now on fine diameter SiC-based fibres were either global (elemental analysis, XRD) or obtained from very restricted parts of the specimens (AES, TEM). The aim of this work was to perform local investigations of the fibres (i) from the bulk, at a micrometer scale, mainly by means of two complementary chemical and structural microprobes: electron probe microanalysis (EPMA) and Raman microspectroscopy (RMS) and (ii) from the surface, at a nanometer scale by Auger electron spectroscopy (AES) and X-ray electron spectroscopy (XPS). The results of the present investigation and previous work from litterature have been discussed on the basis of what is known about their respective preparation process.

2. Experimental

The general properties provided by the manufacturers for the various fibre lots investigated in this study are listed in Table I. It is worth mentioning that some of these fibres were still under development and that their properties may have been improved until now.

Prior to analysis, all the fibres having polymeric coating were desized in a boiling acetone/ethanol mixture and thermally treated at 600°C in high vacuum (residual pressure: 10^{-3} Pa) for one hour.

The morphology and the microstructure of the fibres were characterised by high resolution scanning electron microscopy (SEM) with a Hitachi S-4500 instrument equipped with a field emission gun.

Electron probe microanalysis (EPMA) (SX 100 from CAMECA, France) analyses were conducted on

TABLE I Properties of the SiC-based fibre lots investigated in the present study (general properties from producer's data sheets, chemical composition from literature)

	Hi-Nicalon[1]	Hi-Nicalon S[1]	Tyranno SA[2]	Sylramic[3]	Carborundum[4]
Lot n°	18081	281201	132-B	078001	A-252-175A
Reception date	≤1993	01/1998	09/1998	08/1998	≤1994
Diameter (μm)	14	13	10	10.4	30
Density (gcm^{-3})	2.74	3.0	3.02	3.06	
Tensile strength (GPa)	2.8	2.5	2.84	2.9	1.25
Tensile modulus (GPa)	270	408	303	372	
Fracture strain (%)	1.04	0.63	0.94	0.78	
Chemical composition					
from reference: (wt./at. %)	(6)	(7)	(11)	(8)	
Si	62.4/41.6	68.9/48.7	67.8/47.3–47.9	66.6/46.7	
C	37.1/57.8	30.9/51.0	31.3/50.9–51.7	28.5/46.7	
O	0.5/0.6	0.2/0.2	0.3/0.4	0.8/1.0	
Al	—	—	≤2.0/≤1.4	—	
Ti	—	—	—	2.1/0.9	
B	—	—	—	2.3/4.2	
N	—	—	—	0.4/0.6	
C/Si (at.%)	1.39	1.05	1.08	1.0	

Suppliers : [1]Nippon Carbon Co. Japan, [2]Ube Industries Ltd. Japan, [3]Dow Corning Co. USA, [4]Carborundum Co. USA.

polished cross-sections of fibres. The fibre tows were first coated with a thin Au/Pd deposit to avoid any charging effect under the electron probe, inserted between two steel blades and embedded into epoxy resin. The sample was then cut to reveal the fibres cross section and polished. Connections with silver wax were finally established between the metallic blades and the sample holder to eliminate electrical charges. EPMA measurements were performed in the wavelength dispersion mode, with a thallium acid phthalate (TAP) crystal analyser for Si-K_α and Al-K_α, a large pentaerythritol (LPET) crystal analyser for Ti-K_α and a large multilayer pseudo-crystal analyser (LPC2) (with a high signal/noise intensity ratio) for B-K_α, C-K_α and O-K_α. Monocrystalline SiC, TiO_2, Al_2O_3 and pure B were used as standards. The microprobe analyses were performed either from the core or the near-edge of the fibre or according to linescan measurements along the diameter of the fibre. The electron beam was focused on a single point (point mode), allowing a spatial resolution of 1 to several μm^3, depending on the X-ray emitting volume and therefore the composition of the samples. Fibre specimens of relatively large diameters (as compared to the average values) were sometimes selected to record more points along the same fibre diameter.

Auger electron spectroscopy (AES) was used to determine the elemental composition and, in some cases, the oxidation state of the atoms at the surface of the material. The analyses were performed on tows or individual fibres, flatten and mounted on a small piece of indium foil, which was subsequently set on the sample holder. AES measurements were done with a scanning microprobe (VG Microlab 310-F) equipped with a field emission gun and an Ar^+ ion sputtering gun for depth profiling. The variation of the intensities (peak area mode) of the Auger electron peaks (the KLL-transition for all elements) as a function of the sputtering time was used to plot the semi-quantitative composition-depth profile from the sample surface (sputtering rate reference: Ta_2O_5).

X-ray photo-electron spectroscopy (XPS) analyses (ESCALAB 220 i-XL from VG Scientific equipped with an aluminium monochromatic X-ray source Al-K_α at 1486.6 eV) combined with Ar^+ ion sputtering were performed from the surface of single fibres. The monofilament was mounted on a holed sample holder to avoid any substrate effect on the XPS signal. The excited photoelectrons were detected as a function of their energy by an electrostatic hemispherical sector analyser.

The nature of the crystalline phases present in the different fibres was also studied by X-ray diffraction analysis (XRD) (Cu-K_α, Siemens D5000), directly on fibre tows.

Raman microspectroscopy (RMS) is especially suitable to detect and investigate the structural properties of silicon carbide and free carbon containing materials. RMS analyses (LABRAM 010 from Dilor, France) were conducted on polished cross-section of fibres. The samples used were the same as those for EPMA. The monochromatic excitation source was the 514.5 nm emission line of an Ar^+ laser. The power was kept below 0.5 mW to avoid heating of the sample. The lateral resolution of the laser probe was close to 1 μm and the thickness analysed of the order of one to several hundreds nanometers. Similarly to EPMA, linescan measurements were recorded along the diameter of the fibres.

3. Results and discussion

The chemical composition, as locally assessed by EPMA, either from the core or the edge region of the fibres, is presented in Table II. For given fibre type and location, five to ten point measurements were recorded and the average composition calculated. Although already evidenced in very low amounts in the Sylramic fibre [21], EPMA was unable to detect nitrogen whatever the fibre ($x_N < 0.5 - 1$ at.%). To better show any radial gradient in composition, EPMA linescan measurements along the diameter of fibres were recorded.

TABLE II Average local chemical composition of the SiC based fibres as measured by EPMA (present study)

Fibre type	Composition (wt./at. %)						
	Si	C	O	Al	Ti	B	C/Si (at.)
Hi-Nicalon (edge and core)	62.4/41.6	36.9/57.6	0.7/0.8	—	—	—	1.38
Hi-Nicalon S (edge and core)	68.6/48.5	30.5/50.4	0.9/1.1	—	—	—	1.04
Tyranno SA (edge)	68.0/47.8	31.5/51.8	—	0.5/0.4	—	—	1.08
Tyranno SA (core)	62.9/42.3	36.1/56.8	0.4/0.5	0.6/0.4	—	—	1.34
Sylramic (edge)	65.1/45.5	29.2/47.7	—	—	2.5/1.0	3.2/5.8	1.05
Sylramic (core)	62.9/43.2	30.7/49.2	0.4/0.5	—	2.6/1.1	3.4/6.0	1.14
Carborundum (core)	69.9/49.8	30.1/50.2	—	—	—	—	1.01

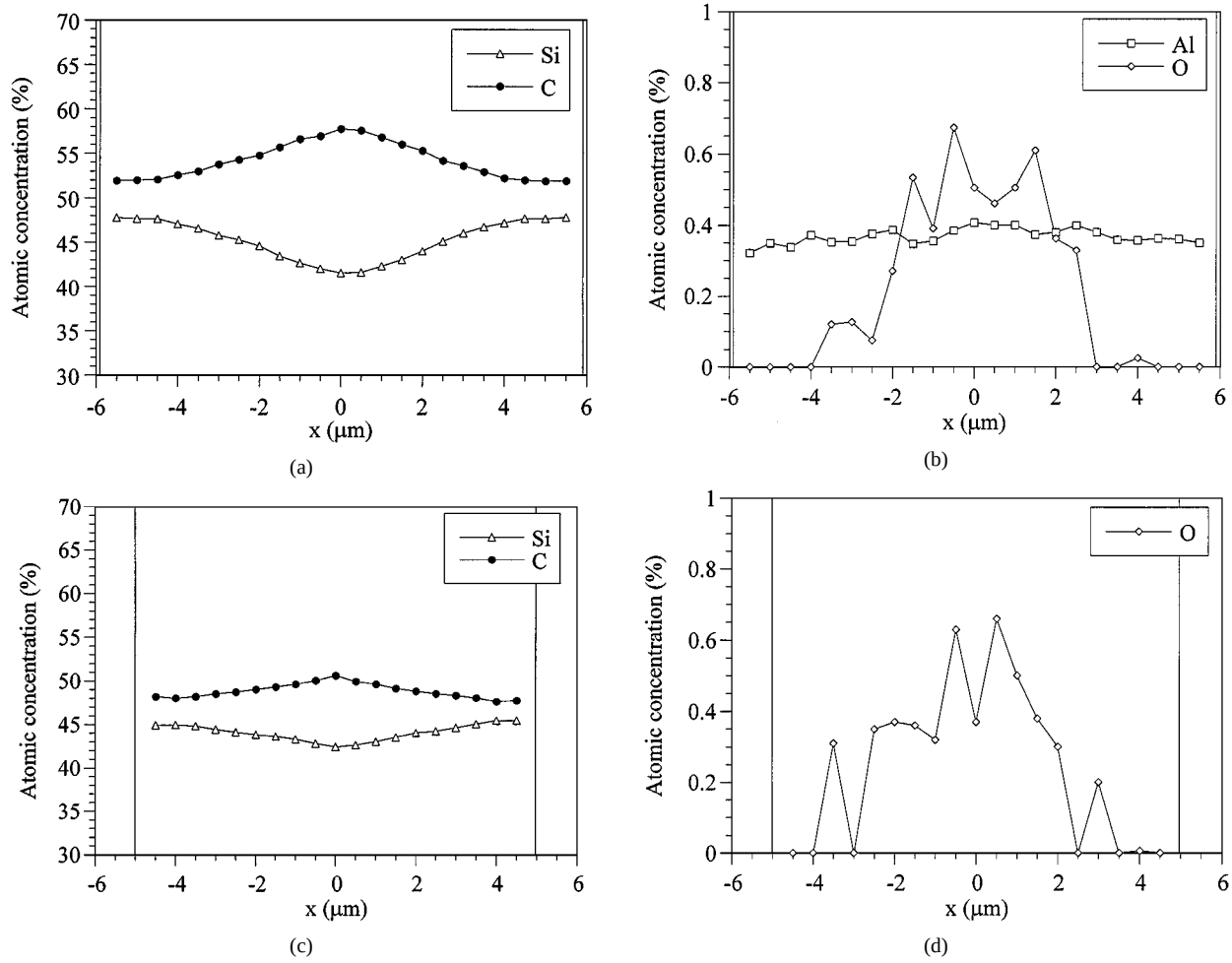

Figure 1 Si, C (a), Al and O (b) atomic concentrations along the diameter of a tyranno SA fibre cross-section, as measured by EPMA. Si, C (c) and O (d) atomic concentration along the diameter of a Sylramic fibre cross-section, as measured by EPMA.

An example of composition profiles for the Tyranno SA and the Sylramic fibres is presented in Fig. 1a–d. The diameter of the two fibres represented in Fig. 1a and b and Fig. 1c and d was respectively 12 μm (a relatively high value as compared to the average for the Tyranno SA fibre) and 10 μm (close to the average for the Sylramic fibre).

When RMS analyses evidenced free carbon within the fibres, the concentration of the free carbon phase (x_{freeC}) was estimated from the EPMA data by considering the presence of SiC, free carbon and other stable secondary phases (e.g., Al_2O_3, Al_4C_3, TiO_2, TiB_2, B_4C. . .), directly inferred from the atomic concentrations and/or supported by complementary techniques (RMS, XRD, AES). The x_{freeC} profiles calculated from Table II and the examples of profiles in Fig. 1 are shown in Fig. 2 together with Hi-Nicalon (14 μm) and Hi-Nicalon S (12 μm) specimens.

The depth composition profiles recorded for the different fibres by AES during ion sputtering are shown in Fig. 3a–e. Only the Si, C and O-KLL Auger electron transitions were considered for the Hi-Nicalon, Hi-Nicalon S and Carborundum fibres. In addition to the Si, C and O atomic concentrations, the Al concentration was also recorded for the Tyranno SA fibre and the Ti and B concentrations for the Sylramic fibre.

The microstructure of the various fibres, as observed from their fracture surfaces by SEM, are shown in

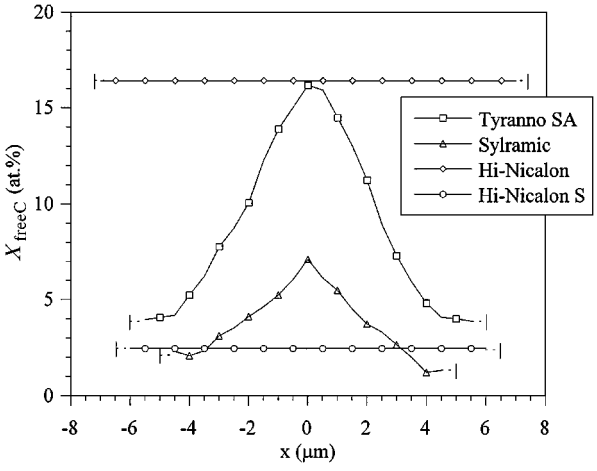

Figure 2 Free carbon concentrations along the diameter of the fibres cross-section, as calculated from EPMA data.

Fig. 4a–e and their XRD respective patterns are represented in Fig. 5.

Average Raman spectra obtained either from the core or the edge regions of the standard and the type S Hi-Nicalon, the Tyranno SA and the Sylramic fibres are shown in Fig. 6a–f. The Fig. 7a–d show the Raman spectra recorded respectively for an average spot, a free carbon rich and a boron carbide rich spot within the Carborundum fibre and a reference spectrum obtained for a B_4C standard.

The Raman spectra recorded from the core of the Hi-Nicalon, Hi-Nicalon type S, Tyranno SA and Sylramic fibres are in good agreement with those previously reported by Colomban on similar materials [27]. They show two intense peaks at about 1350 and 1600 cm^{-1} and an additional weak peak at about 1620 cm^{-1} (Fig. 6a–c, 6e). These bands correspond to the typical vibration modes encountered in low ordered carbon materials (e.g., turbostratic carbon) and graphite. The 1600 cm^{-1} peak (1585 cm^{-1} for highly oriented pyrolytic graphite) with the E_{2g} symmetry (G peak), is characteristic of graphite single crystal. It corresponds to a vibrational mode involving displacements of carbon atoms strongly bonded within the graphene sheets. The two other peaks at 1350 cm^{-1} (D peak) and 1620 cm^{-1} (D′ peak) are observed together with a broadened G peak in polycrystalline or unorganised carbons [28–31].

The occurrence of such features in the Raman spectra clearly indicates that free carbon is present in the bulk of all the polymer-derived fibres.

While invisible (except a slight broad band around 850–900 cm^{-1}) on the spectrum of the Hi-Nicalon fibre (Fig. 6a), two narrow peaks at 796 and 972 cm^{-1} are visible for the Hi- Nicalon S, Tyranno SA and Sylramic fibres (Fig. 6b–f) [27]. Those features are respectively assigned to the transverse optic (TO) and the longitudinal optic (LO) modes for the 3C-SiC phase [32].

Similarly to the EPMA, RMS linescan analyses along the diameter of the various fibres were carried out. Again, for comparison, the free carbon to SiC peak intensity ratio (I_{1600}/I_{796}), which gives an indication of the evolution of the free carbon content along the diameter, is shown in Fig. 8 for Hi-Nicalon S, Tyranno SA and Sylramic fibres. The diameters of the fibres investigated by RMS were respectively 13 μm, 10 μm and 9.5 μm, i.e., close or slightly lower than the average value.

3.1. Standard and type S Hi-Nicalon fibres

The microstructure of the Hi-Nicalon and Hi-Nicalon S fibres is fine and homogeneous (Fig. 4a and b). Nanometer-sized grains are easily observable in the Hi-Nicalon S fibre, while hardly discernible in the Hi-Nicalon fibre.

The main phase is β-SiC (3C) for both the Hi-Nicalon and Hi-Nicalon S fibres (111 reflection at $2\theta = 35.7°$, 220 at $2\theta = 60.0°$ and 311 at $2\theta = 72.0°$) (Fig. 5a and b). A weak peak characteristic of the α-phase is also visible at $2\theta = 34.2°$. It was assigned to 111 stacking faults within the β-SiC structure. The diffraction peaks for the Hi-Nicalon S fibre are significantly sharper and more intense than those for the Hi-Nicalon fibre. Such XRD features clearly confirm the better crystalline character of the former fibre compared to the latter.

The EPMA and RMS microprobe analyses revealed homogeneous elemental and phase compositions along both fibre diameters (Figs 2 and 8). The chemical composition derived from the present EPMA measurements is in excellent agreement with the data reported by NC and other authors [9–16]. While the C/Si atomic ratio is much greater than 1 in the Hi-Nicalon fibre, it is 1.04 for Hi-Nicalon S fibre, i.e., nearly stoichiometric. The presence of an oxygen and carbon rich surface layer is a common characteristic of all these fibres, as shown on the AES profiles (Fig. 3a–e). The carbon layer is extremely thin (about 20 nm) for the Hi-Nicalon fibre (Fig. 3a). It rapidly vanishes after sputtering, the composition becoming constant, with values in rather good agreement with the EPMA bulk analyses. The carbon rich surface layer is much thicker for the Hi-Nicalon S fibre (about 80 nm) and also contains some oxygen (Fig. 3b). As expected for both fibres, the major phase is 3C (or β)-SiC as shown by XRD analyses. Although the Hi-Nicalon S is almost pure SiC, some residual oxygen ($\approx$1 at.%) as well as some free turbostratic carbon ($C_{free} \approx 2.5$ at.%) are still present in this fibre.

The mechanism of the pyrolysis involved in the Hi-Nicalon fibre manufacturing has been studied into details [33]. The pyrolysis in an argon flow of the electron beam-cured (EB) filaments results in a first evolution of H_2 and CH_4 generated from the decomposition of the Si-H and Si-CH_3 bonds of the PCS at about 550–950°C, followed by a H_2 evolution resulting from the cleavage of the C-H bonds of the Si-CH_2-Si chains around 750–1400°C [33]. In addition to the cross-linking of the PCS chains, ethylene groups are likely to be formed by free radical reactions during the first pyrolysis step. The C=C bonds trapped within the three-dimensional network subsequently generate aromatic carbon as basic structural units, finally coalescing into the free carbon phase.

Tazi-Hemida *et al.* showed that the pyrolysis up to 1000°C in a hydrogen flow of experimental PCS-based EB-cured fibres is an efficient way to reduce the free carbon content of the resulting ceramic fibres [34].

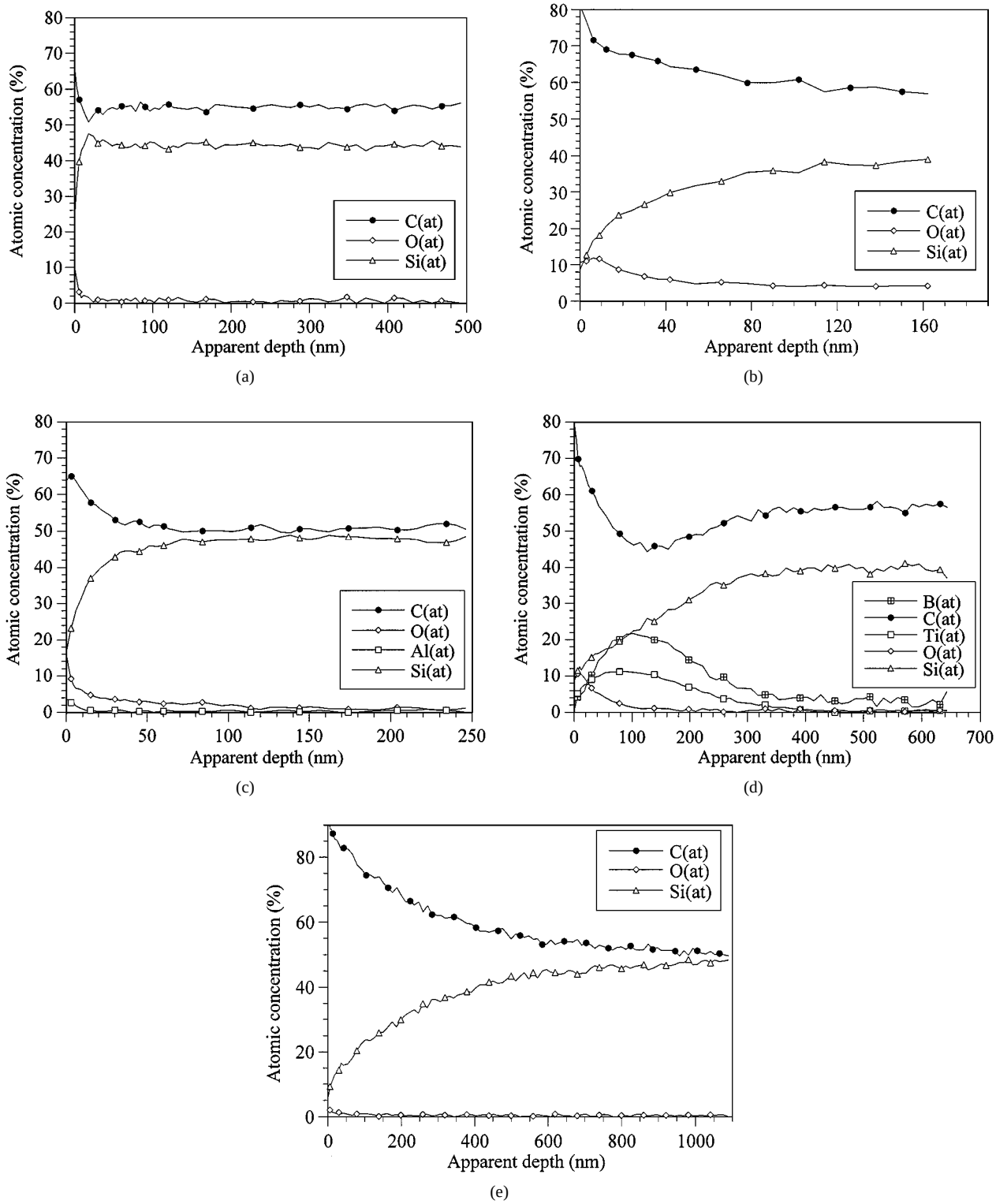

Figure 3 AES depth profiles recorded from the surface of the Hi-Nicalon (a), Hi-Nicalon S (b), Tyranno SA (c), Sylramic (d) and Carborundum fibre (e) (sputtering rate reference Ta_2O_5).

The ceramic obtained at 1000°C is still amorphous and highly hydrogenated but the hydrogen release and the SiC crystallisation are simply achieved through a further heat treatment in argon. More recently, Takeda *et al.* from Nippon Carbon described the effect of a hydrogen atmosphere on the pyrolysis of similar EB-cured PCS fibre batches as those used for the processing of the Hi-Nicalon fibres [35]. While the PCS demethanation (from the breaking of methyl groups) is only partial during the pyrolysis of the PCS in argon, it is favoured (and the dehydrogenation unfavoured) in a hydrogen atmosphere and therefore results in a significantly lower free carbon amount. It is anticipated that some similar process is employed in the manufacturing of Hi-Nicalon S type fibre, i.e., a continuous pyrolysis of the filaments in a reducing atmosphere (hydrogen-based), followed by a heat exposure up to a higher temperature in an inert atmosphere to stabilise the fibre.

Under such processing conditions, the C/Si ratio of the final ceramic fibre is set from the early pyrolysis

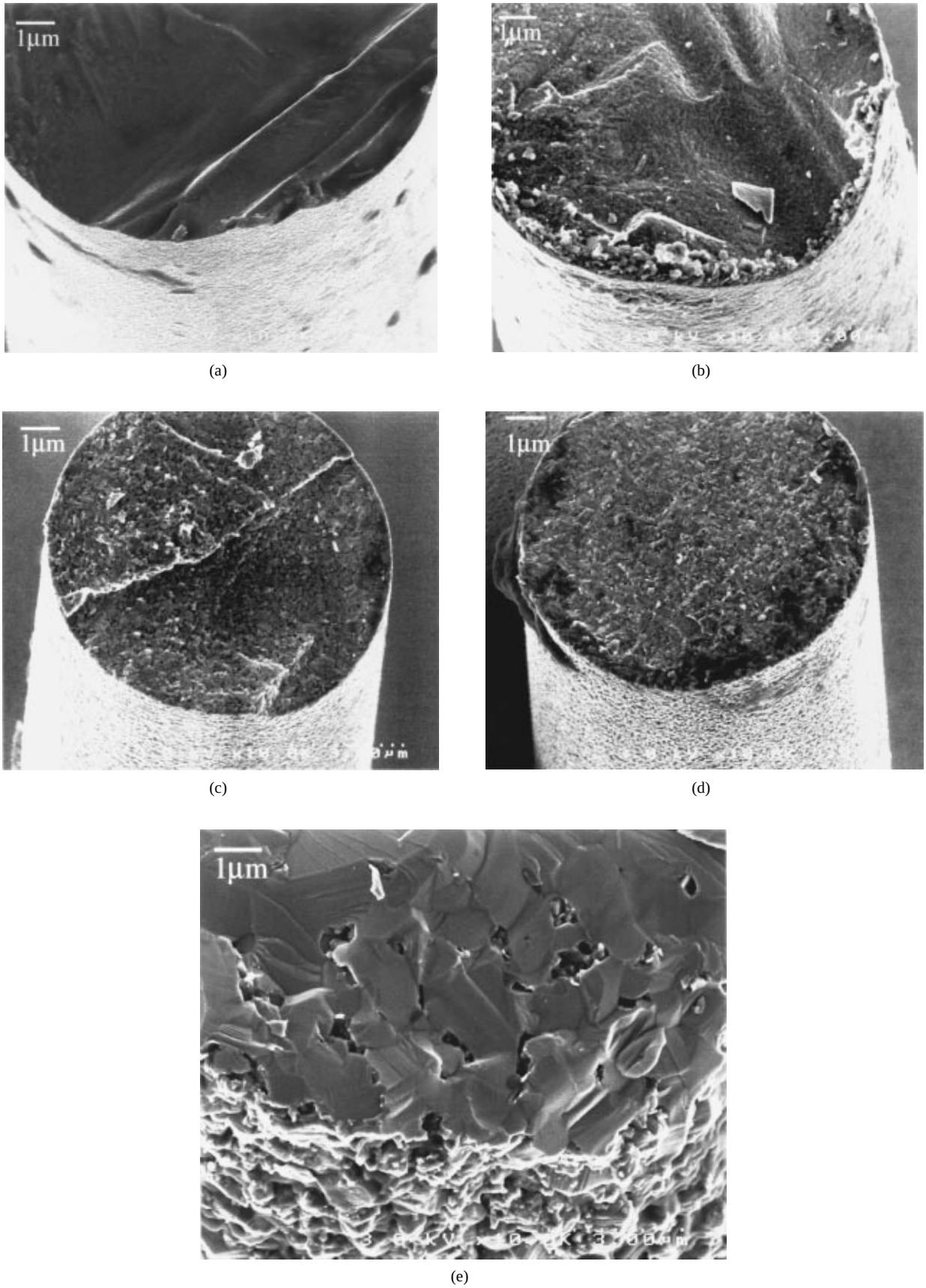

Figure 4 SEM micrographs of the fracture surface of the Hi-Nicalon (a), Hi-Nicalon S (b), Tyranno SA (c), Sylramic (d) and Carborundum fibre (e).

(400–800°C). Within that temperature range, the preceramic material is still nanoporous and its density rather low. Such a porous microstructure, as well as a low heating rate would allow hydrocarbon species to migrate freely throughout the fibre outward [36]. The pyrolysis of the standard and type S Hi-Nicalon fibres is therefore equally achieved and the C/Si ratio set almost constant within the whole fibres (as shown by EPMA and RMS) before the final densification at higher temperature. The CO and SiO evolution being almost

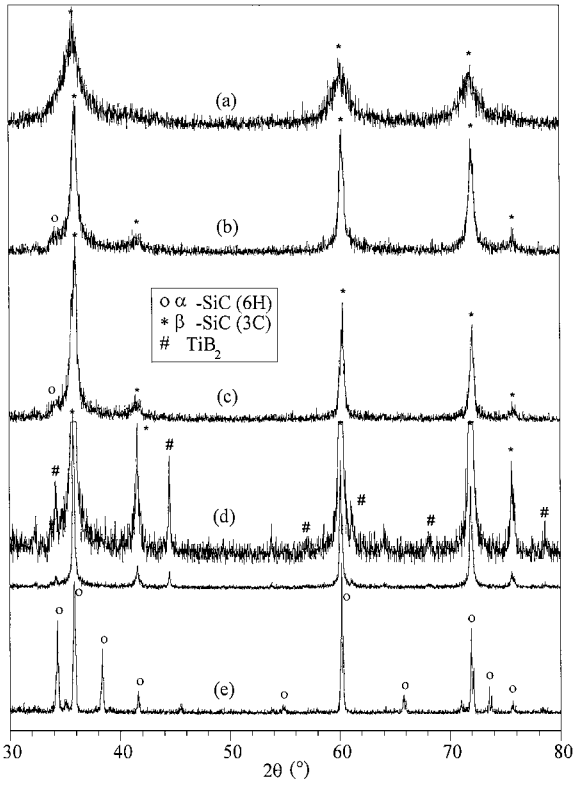

Figure 5 X-ray diffraction patterns of the Hi-Nicalon (a), Hi-Nicalon S (b), Tyranno SA (c), Sylramic (d) and Carborundum fibre (e).

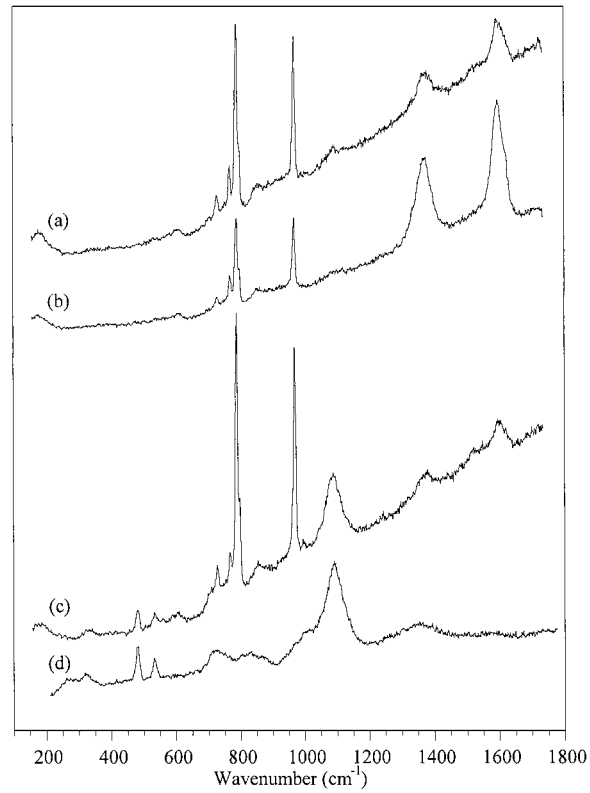

Figure 7 Raman spectra of the Carborundum fibre. (a) average, (b) carbon rich and (c) boron carbide rich spots within the fibre and (d) boron carbide standard.

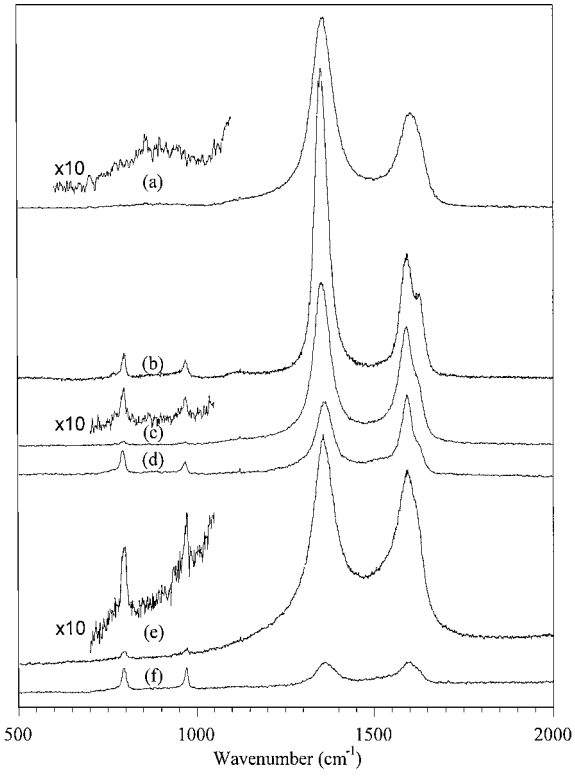

Figure 6 Raman spectra of the Hi-Nicalon core (a), Hi-Nicalon S core (b), Tyranno SA core (c) and edge (d) and Sylramic fibre core (e) and edge (f).

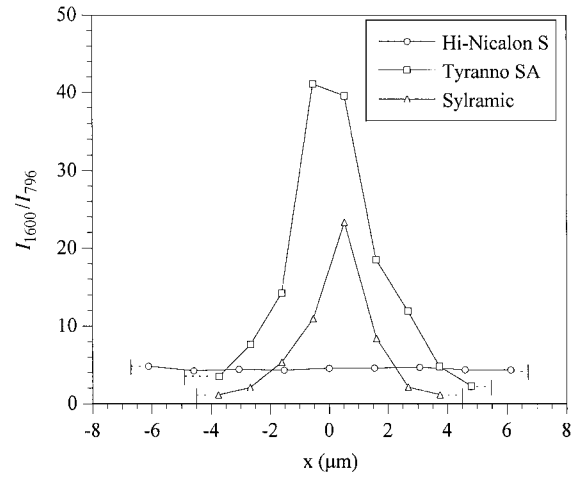

Figure 8 Free carbon to SiC peak intensity ratio (I_{1600}/I_{796}) along the diameter of the fibres cross-section, as measured by RMS.

suppressed in the oxygen free process, the final stage of the pyrolysis ($\leq$1400°C) occurs with a hydrogen formation only and without any further change of the C/Si ratio.

3.2. Sylramic and Tyranno SA fibres

The Tyranno SA and the Sylramic fibres display relatively coarse grains (up to 100–200 nm in size) (Fig. 4c and d). It is worthy of note that the edge region of both fibres is apparently more crystalline than the core, whose microstructure is rather finer grained and porous.

Similarly to the previous fibres, the main phase present in the Tyranno SA and Sylramic fibres is a slightly faulted β-SiC (3C) phase (Fig. 5c and d). Again, the sharp XRD peaks observed for the two fibres clearly confirmed the larger SiC crystallite size than that of the Hi-Nicalon fibre. It is worthy of note that peaks characteristic of the TiB_2 phase are also clearly visible for the

Sylramic fibre, as already mentionned by other authors [21, 22].

In a similar manner, both EPMA (from phase calculations) and RMS (from direct measurement) data evidenced that the Sylramic and the Tyranno SA fibres still contain some free carbon, as previously shown by Colomban through RMS analyses [27] and by Berger *et al*. through transmission electron microscopy investigations (TEM) [37]. However, these two fibres show some original features in chemical and phase compositions when compared to the NC fibres. The nearly stoichiometric SiC composition observed at their edge ($x_{\text{freeC}} \approx 2$ at.% for the Sylramic fibre and ≈4 at.% for the Tyranno SA fibre) becomes significantly richer in free carbon while moving to the core (e.g., respectively $x_{\text{freeC}} \approx 7$ at.% and ≈16 at.% in Fig. 2). Although some variations in x_{freeC} were sometimes observed in the core of individual fibres, the occurrence of a free carbon rich core was generally observed for all fibres from both types. Furthermore, besides the x_{freeC} radial gradient, very low amounts of oxygen (≈0.5 at.%) exist within their cores while both fibre edges are totally oxygen free (Fig. 1b and d). Aluminium (≈0.4 at.%) was also found homogeneously distributed within the Tyranno SA fibre (Fig. 1d). The surface layer of the Tyranno SA fibre not only involves carbon and oxygen but also some aluminium, concentrated at the surface of the fibre (Fig. 4c). The aluminium was found in the oxide state (i.e., Al_2O_3) from the analysis of the kinetic energy of the Al-KLL Auger electrons, as well as from the value of the maximum energy of the Al_{kl1} XPS peak (74.0 eV). The thickness of this alumina rich surface layer is about 20 nm. Titanium (≈1 at.%) as well as boron (≈6 at.%) were also found homogeneously distributed along the diameter of the Sylramic fibre (although not shown in Fig. 1). The depth profile composition recorded for the Sylramic fibre is relatively complex (Fig. 3d). The carbon and oxygen concentrations gradually decrease, while the boron and titanium contents increase, from the surface of the fibre, to a depth of about 80 nm. The boron and titanium rich region forms a 300 nm thick layer covering the fibre. The XPS spectra recorded for the Sylramic fibre showed a B^{1s} peak of maximum energy 187.5 eV and a $Ti^{2p}_{3/2}$ peak maximum energy of 454.6 eV. The latter peak position corresponds rather well to that reported for titanium environment in TiB_2 [38], according to XRD and TEM analyses [21, 22]. Because the energy level of the B^{1s} peak measured is very close to those corresponding to the chemical bonding of boron in both B_4C [39] or TiB_2 [38], B_4C could not be evidenced by XPS. However, the excess of boron with respect to the TiB_2 composition, which has been shown by both EPMA and XPS surface analysis, can be assigned to boron carbide.

A relationship was found between the I_{1600}/I_{796} profiles determined from RMS and the C_{free} profiles estimated from EPMA (Figs 2 and 8), giving again clear indication of the free carbon radial gradient throughout the Sylramic and the Tyranno SA fibres. Additionally, as visible from the sharpening of the Raman peaks, the crystallinity of both the β-SiC and the free carbon phases increases simultaneously from the core to the edge of the two fibres. The free carbon excess of the fibre core with regard to the surface, was also pointed out by Colomban for the Tyranno SA whereas no difference was found between the core and the surface of the Sylramic fibre [27].

Similarly to the first polycrystalline fibres developed by Dow Corning Co. [40–43], the Sylramic and Tyranno SA fibres seem to be prepared according to a more or less common strategy consisting in reaching the SiC stoichiometry through the carbothermal reduction of a Si-C-O type fibre, while preventing exaggerated crystal growth and voids formation [19–22]. Such particular conditions are achieved by the incorporation of a sintering aid, i.e., boron (the DC route) or aluminium (the Ube route) into the precursor Si-C-O fibre or during the subsequent processing steps.

The processing route to the Sylramic fibre has not been disclosed [21]. However, this fibre might be prepared according to one of the Dow Corning Co. patents. Deleeuw *et al*. described a process in which polycrystalline SiC fibres are prepared through the infusibilisation and boron addition (with NO and BCl_3) of PCS green fibres prior to ceramisation [40]. An alternative route proposed by Lipowitz *et al*. describes the incorporation of boron at high temperature during ceramisation [43]. Some process related to the heat treatment up to 1800°C under argon of a Si-Ti-C-O Tyranno Lox-M type fibre in presence of B_2O_3 (example 7, [43]) for instance, might be involved for the Sylramic fibre preparation.

The Tyranno SA is an evolution of the various polymetallocarbosilane-based fibres developed by Ube [20]. The Si-C-O fibre precursor is in this case a Si-Al-C-O fibre (so called AM fibre). The polyaluminocarbosilane (PACS) polymer precursor is prepared by the reaction of a PCS with aluminiumacetylacetonate. The PACS is melt spun into filaments and cured in air. The Si-Al-C-O fibres obtained are subsequently converted into the Tyranno SA fibre, by decomposition with an evolution of CO and SiO ($1500 < T < 1700$°C) and sintering ($T \geq 1800$°C).

Because it is governed by gases (CO and SiO) diffusion outward, the carbothermal reduction of Si-C-O Nicalon type fibres proceeds from the surface to the fibre core, resulting in a steep gradient of composition and microstructure also called skin/core effect [3, 4, 8, 44]. A crystallised SiC scale resulting from the superficial degradation is indeed generally observed. The decomposition of the fibre and the thickness of the skin both improve with the reaction rate (with time and temperature), gradually reaching the fibre core. Although the presence of sintering aids and the careful optimisation of the carbothermal reduction/sintering process [41], such a skin/core mechanism, might also be involved during the heat treatment of the Sylramic and the Tyranno SA fibre and might explain the structure and composition gradient evidenced by EPMA and RMS, for the specific fibre lots analysed in the present study. As the decomposition gradually proceeds, the SiC scale might become sufficiently thick and tight (owing to the starting sintering) to prevent (or slow down) the gas diffusion outward. This phenomenon, might

therefore modify the inner CO and SiO partial pressures at a level favouring the elimination of oxygen as SiO and the formation of some free carbon residue. The sintering of the fibres is likely to start before the completion of the carbothermal reduction. Because of its stoichiometric composition, the edge of the fibres first sinters and densifies whereas the free carbon located at the grain boundary might prevent SiC sintering within the core. Even at the end of the high temperature treatment, the sealed outer part of the fibre might prevent the complete release of SiO and CO. Very low amounts of silicon oxycarbide therefore still remain within the core, stabilised by the high free surface of the inner finer-grained SiC.

The chemical and structural radial gradients for both Tyranno SA and Sylramic fibres may appear surprising (they have not been reported so far and they fairly disagree with data from literature) [19–22, 26]. The free carbon radial gradient may vary with fibre lots and the manufacturer processing conditions which may have been changing for the past few years. Hence, Xu *et al*. showed that boron doped Si-C-O fibres with inadequate oxygen concentration may yield free carbon rich SiC-based fibres after heat treatment, whereas Si-C-O fibres of optimal composition give rise to stoichiometric SiC at a depth of at least 0.5 μm as shown by AES [41]. Very recently, Ishikawa *et al*. showed that large diameter Tyranno SA fibres (11 μm) generally exhibit a porous core due to an incomplete conversion to SiC (suggesting a free carbon excess), whereas thinner fibres (8 μm) rather tend to be dense and probably near stoichiometric [45]. If one considers that such a porous and not fully converted/sintered core microstructure might be related to residual free carbon, this feature would support the occurrence of the chemical gradient which has been evidenced by EPMA on a relatively large diameter Tyranno SA fibre (12 μm) (Fig. 2).

3.3. Carborundum fibre

The Carborundum fibre obviously exhibits a much coarser microstructure than all other fibres. Large micrometer-sized grains as well as an abundant intergranular porosity are clearly visible in that fibre (Fig. 4e).

The α-phase and more especially the 6H-SiC polytype prevails in the Carborundum fibre, as shown on the XRD spectrum (10.1 reflection at $2\theta = 34.2^\circ$, 10.2 at $2\theta = 35.7^\circ$, 10.3 at $2\theta = 38.2^\circ$, 11.0 at $2\theta = 60.2^\circ$ and 11.6 at $2\theta = 72.0^\circ$) (Fig. 5e). The α-SiC diffraction peaks are particularly sharp, in agreement with the large grain size evidenced by SEM.

The fibre is oxygen free and has the closest C/Si ratio to SiC stoichiometry (Table II). However, although not mentioned in Table II, small boron rich spots were randomly detected by EPMA, which might arise from boron carbide inclusions [46].

The Raman spectra show original features while compared to the polymer-based fibres (Fig. 7a–c). The free carbon characteristic peaks at 1350 and 1600 cm^{-1} are still present but have much lower intensities. The SiC features are also more complex with sharp and intense α-SiC characteristic peaks at 729, 768, 789 and 970 cm^{-1} attributed to (a) non-cubic polytype(s) including mainly 6H [32]. The stoichiometric character of the fibre is obvious in that free carbon is almost absent, at least, for most of the RMS point analyses (Fig. 7a). However, the fibre composition within the cross section may not be always homogeneous. Few free carbon rich spots are sometimes evidenced (Fig. 7b), which are generally associated with the microporosities. Several weak peaks at 320, 480, 535 and 1080 cm^{-1} also seldom appear on the Raman spectra recorded from very restricted spots (Fig. 7c), which were assigned to boron carbide B_4C (Fig. 7d) [47]. B_4C inclusions are invariably associated with a very weak free carbon content (Fig. 7c).

The Carborundum fibre is fabricated according to a process totally different from those of the polymer-derived fibres. The green fibre is prepared by the extrusion of a sinterable α-SiC powder mixed with a polymer binder [23, 24]. A continuous sintering process was developed to convert the green fibre into a dense polycrystalline SiC fibre. The sinterable SiC powder also contains free carbon and boron additives. Free carbon is added to remove traces of silica at relatively low temperatures (about 1300–1400°C) in order to avoid any exaggerated SiC grain growth preventing sintering. Some traces of the carbon additive still remain in the sintered fibres. Because they were initially present at the grain boundary, they are generally still located near large pores, as observed by RMS. Boron is added as a sintering aid. It is also seldom detected by RMS as B_4C inclusions probably generated at high temperature [46]. By reference to the sintering of micrometre size α-SiC powders in the processing of conventional monolithic SiC ceramics, it is assumed that the sintering of such a fibre has been performed at a very high temperature, a feature which would explain its high crystalinity and creep resistance.

4. Conclusion

Although containing some residual oxygen ($\approx$1 at. %) and free carbon ($\approx$2 at. %), the Hi-Nicalon type S fibre has a homogeneous near stoichiometric composition. The Tyranno SA and the Sylramic fibres have also a near stoichiometric composition but it is only effective near the edge region, the core still containing some free carbon (e.g., up to $\approx$14 at. % and $\approx$6 at. % respectively in some fibres). The composition of the Carborundum fibre is very close to stoichiometric SiC except few free carbon or boron carbide inclusions.

The composition and microstructure features of the fibres arise from their respective processing routes. The free carbon of the NC fibres is influenced by the atmosphere of the PCS-pyrolysis occurring at moderate temperatures (500–1000°C). Under such conditions, the composition is set throughout the fibre before the final densification at high temperature. Hence, if the atmosphere is adequate (in terms of hydrogen partial pressure), the fibre may have an homogeneous stoichiometric composition. The composition and the microstructure of the Sylramic and Tyranno SA fibres

seem to be governed by the carbothermal reduction of silicon oxycarbide in presence of free carbon beyond 1500°C. Such a mechanism is highly conditioned by the diffusion of SiO and CO outward. The reaction starts at the surface and then gradually reaches the fibre core, while the material is starting to densify. Under certain conditions (e.g., fibres or relatively large diameters), this process seems to yield a significant radial gradient of composition and microstructure.

Acknowledgements

This work was supported by CNRS and the Chinese Academy of Sciences through a grant given to Dr. Dong Shaoming and by SNECMA Moteurs. The authors would like to thank Nippon Carbon Co. Ltd., Ube Industries Ltd., Dow Corning Co. and Carborundum Co. for their supply of the SiC fibres.

References

1. C. LAFFON, A. M. FLANK, P. LAGARDE, M. LARIDJANI, R. HAGEGE, P. OLRY, J. COTTERET, J. DIXMIER, J. L. MIQUEL, H. HAMMEL and A. P. LEGRAND, *J. Mater. Sci.* **24** (1989) 1503.
2. L. PORTE and A. SARTRE, *ibid.* **24** (1989) 271.
3. P. LE COUSTUMER, M. MONTHIOUX and A. OBERLIN, *J. Eur. Ceram. Soc.* **11** (1993) 95.
4. T. MAH, N. LECHT, D. E. Mc CULLUM, J. R. HOENIGMAN, H. M. KIM, A. P. KATZ and H. A. LIPSITT, *J. Mater. Sci.* **19** (1984) 1191.
5. S. M. JOHNSON, R. D. BRITTAIN, R. H. LAMOREAUX and D. J. ROWCLIFFE, *J. Amer. Ceram. Soc.* **71** (1988) C132.
6. T. J. CLARK, M. JAFFE, J. RABE and N. R. LANGLEY, *Ceram. Eng. and Sci. Proc.* **7**(7/8) (1986) 901.
7. B. A. BENDER, J. S. WALLACE and D. J. SCHRODT, *J. Mater. Sci.* **26** (1991) 970.
8. R. BODET, N. JIA and R. E. TRESSLER, *J. Eur. Ceram. Soc.* **16** (1996) 653.
9. M. TAKEDA, Y. IMAI, H. ICHIKAWA, T. ISHIKAWA, T. SEGUSHI and K. OKAMURA, *Ceram. Eng. and Sci. Proc.* **12**(7/8) (1991) 1007.
10. M. TAKEDA, Y. IMAI, H. ICHIKAWA, T. ISHIKAWA, N. KASAI, T. SEGUSHI and K. OKAMURA, *ibid.* **13**(7/8) (1992) 209.
11. M. TAKEDA, Y. IMAI, H. ICHIKAWA, N. KASAI, T. SEGUSHI and K. OKAMURA, *ibid.* **14**(9/10) (1993) 540.
12. G. CHOLLON, R. PAILLER, R. NASLAIN, F. LAANANI, M. MONTHIOUX and P. OLRY, *J. Mater. Sci.* **32** (1997) 327.
13. M. TAKEDA, J. SAKAMOTO, Y. IMAI, H. ICHIKAWA and T. ISHIKAWA, *Ceram. Eng. and Sci. Proc.* **15**(4) (1994) 133.
14. M. TAKEDA, J. SAKAMOTO, A. SAEKI, Y. IMAI and H. ICHIKAWA, *ibid.* **16**(4/5) (1995) 37.
15. M. TAKEDA, J. SAKAMOTO, A. SAEKI and H. ICHIKAWA, *ibid.* **17**(4) (1996) 35.
16. H. ICHIKAWA, M. TAKEDA and T. NODA, in "Ceramic Material Systems with Composite Structures, Ceramic Transactions," Vol. 99, edited by N. Takeda, L. M. Sheppard and J. Kon, (The Am. Ceram. Soc., Westerville Ohio, USA, 1998) p. 109.
17. T. YAMAMURA, S. MASAKI, T. ISHIKAWA, M. SATO, M. SHIBUYA and K. KUMAGAWA, *Ceram. Eng. and Sci. Proc.* **17**(4) (1996) 184.
18. K. KUMAGAWA, H. YAMAOKA, M. SHIBUYA and T. YAMAMURA, *ibid.* **19**(3) (1998) 65.
19. T. ISHIKAWA, Y. KOHTOKU, K. KUMAGAWA, T. YAMAMURA and T. NAGASAWA, *Nature* **391** (1998) 773.
20. T. NAKAYASU, M. SATO, T. YAMAMURA, K. OKAMURA, Y. KATOH and K. KOHYAMA, *Ceram. Eng. and Sci. Proc.* **20**(4) (1999) 301.
21. J. LIPOWITZ, J. A. RABE, A. ZANGVIL and Y. XU, *ibid.* **18**(3) (1997) 147.
22. H. M. YUN and J. A. DI CARLO, *ibid.* **20**(4) (1999) 259.
23. F. FRECHETTE, B. DOVER, V. VENKATESWARAN and J. KIM, *ibid.* **12**(7/8) (1991) 992.
24. J. J. BIERNACKI, V. VENKATESWARAN and M. ANDREJCACK, *ibid.* **18**(3) (1997) 73.
25. J. A. DI CARLO, *Comp. Sci. and Tech.* **51**(2) (1994) 213.
26. Committee on Advanced Fibers for High Temperature Ceramic Composites, "Ceramic Fibers and Coatings" (National Academy Press , Washington D.C., 1998).
27. P. COLOMBAN, American Ceramic Society Annual Meeting, Indianapolis, April 24–28 1999.
28. F. TUINSTRA and J. L. KOENIG, *J. Chem. Phys.* **53** (1970) 1126.
29. I. POCSIK, M. HUNDHAUSEN, M. KOOS and L. LEY, *J. Non-Cryst. Solids* **223**(1–3) (1998) 1083.
30. M. J. MATTHEWS, M. A. PIMENTA, G. DRESSELHAUS and M. ENDO, *Phys. Rev. B* **59**(10) (1999) R6585.
31. P. LESPADE, A. MARCHAND, M. COUZI and F. CRUÈGE, *Carbon* **22**(4/5) (1984) 375.
32. H. OKAMURA, E. SAKUMA, J. H. LEE, H. MUKAIDA, S. MISAWA, K. ENDO and S. YOSHIDA, *J. Appl. Phys.* **61** (1987) 1134.
33. M. SUGITOMO, T. SHIMOO, K. OKAMURA and T. SEGUSHI, *J. Amer. Ceram. Soc.* **78**(4) (1995) 1013.
34. A. TAZI HEMIDA, R. PAILLER and R. NASLAIN, *J. Mater. Sci.* **32** (1997) 2359.
35. M. TAKEDA, A. SAEKI, J. I. SAKAMOTO, Y. IMAI and H. ICHIKAWA, *J. Amer. Ceram. Soc.* **83**(5) (2000) 1063.
36. K. OKAMURA, T. SHIMOO, I. TSUKADA and T. SEGUSHI, in "Ceramic Material Systems with Composite Structures, Ceramic Transactions," Vol. 99, edited by N. Takeda, L. M. Sheppard and J. Kon (The American Ceramic Society, Westerville-Ohio, USA, 1998) p. 101.
37. M. H. BERGER, N. HOCHET and R. A. BUNSELL, *Ceram. Eng. and Sci. Proc.* **19**(3) (1998) 39.
38. E. C. ONYIRIUKA, *Appl. Spectrosc.* **47**(1) (1993) 35.
39. S. JACQUES, A. GUETTE, X. BOURRAT, F. LANGLAIS, C. GUIMON and C. LABRUGÈRE, *Carbon* **34**(9) (1996) 1135.
40. D. C. DELEEUW, J. LIPOWITZ and P. P. LU, US Pat. No. 5071600, Dec. 10 1991 and US Pat. No. 5162269, Nov. 10 1992.
41. Y. XU, A. ZANGVIL, J. LIPOWITZ, J. A. RABE and G. A. ZANK, *J. Amer. Ceram. Soc.* **76**(12) (1993) 3034.
42. J. LIPOWITZ, T. BARNARD, D. BUJALSKI, J. A. RABE, G. A. ZANK, A. ZANGVIL and Y. XU, *Comp. Sci. and Tech.* **51** (1994) 167.
43. J. LIPOWITZ and J. A. RABE, US Pat. No. 5279780, Jan. 18 1994 and US Pat. No. 5366943, Nov. 22 1994.
44. O. DELVERDIER, M. MONTHIOUX, D. MOCAER and R. PAILLER, *J. Eur. Ceram. Soc.* **12** (1993) 27.
45. T. ISHIKAWA, S. KAJII and T. HISAYUKI, Annual Cocoa Beach Conference & Exposition, Cocoa Beach, Jan. 23–28 2000.
46. H. TENAILLEAU, X. BOURRAT, R. NASLAIN, R. E. TRESSLER and L. A. GIANUZZI, *J. Amer. Ceram. Soc.* **81**(8) (1998) 2037.
47. D. R. TALLANT, T. L. ASELAGE, A. N. CAMPBELL and D. EMIN, *Phys. Rev.* **10**(8) (1989) 5649.

Received 26 July
and accepted 28 November 2000